



## OPEN ACCESS

## EDITED BY

Silvia Capuani,  
National Research Council (CNR), Italy

## REVIEWED BY

Matthias J. Bahr,  
University Hospital Rupp-  
Brandenburg, Germany  
Michael D. Noseworthy,  
McMaster University, Canada

## \*CORRESPONDENCE

Marian A. Troelstra,  
mtroelstra@hotmail.com

## SPECIALTY SECTION

This article was submitted to  
Computational Physiology and  
Medicine,  
a section of the journal  
Frontiers in Physiology

RECEIVED 17 May 2022

ACCEPTED 27 July 2022

PUBLISHED 06 September 2022

## CITATION

Troelstra MA, Van Dijk A-M, Witjes JJ,  
Mak AL, Zwirs D, Runge JH, Verheij J,  
Beuers UH, Nieuwdorp M,  
Holleboom AG, Nederveen AJ and  
Gurney-Champion OJ (2022), Self-  
supervised neural network improves tri-  
exponential intravoxel incoherent  
motion model fitting compared to least-  
squares fitting in non-alcoholic fatty  
liver disease.  
*Front. Physiol.* 13:942495.  
doi: 10.3389/fphys.2022.942495

## COPYRIGHT

© 2022 Troelstra, Van Dijk, Witjes, Mak,  
Zwirs, Runge, Verheij, Beuers,  
Nieuwdorp, Holleboom, Nederveen and  
Gurney-Champion. This is an open-  
access article distributed under the  
terms of the [Creative Commons  
Attribution License \(CC BY\)](https://creativecommons.org/licenses/by/4.0/). The use,  
distribution or reproduction in other  
forums is permitted, provided the  
original author(s) and the copyright  
owner(s) are credited and that the  
original publication in this journal is  
cited, in accordance with accepted  
academic practice. No use, distribution  
or reproduction is permitted which does  
not comply with these terms.

# Self-supervised neural network improves tri-exponential intravoxel incoherent motion model fitting compared to least-squares fitting in non-alcoholic fatty liver disease

Marian A. Troelstra<sup>1\*</sup>, Anne-Marieke Van Dijk<sup>2</sup>, Julia J. Witjes<sup>2</sup>,  
Anne Linde Mak<sup>2</sup>, Diona Zwirs<sup>2</sup>, Jurgen H. Runge<sup>1</sup>,  
Joanne Verheij<sup>3</sup>, Ulrich H. Beuers<sup>4</sup>, Max Nieuwdorp<sup>2</sup>,  
Adriaan G. Holleboom<sup>2</sup>, Aart J. Nederveen<sup>1</sup>  
Oliver J. Gurney-Champion<sup>1</sup>

<sup>1</sup>Department of Radiology and Nuclear Medicine, Amsterdam UMC, Amsterdam, Netherlands,

<sup>2</sup>Department of Vascular Medicine, Amsterdam UMC, Amsterdam, Netherlands, <sup>3</sup>Department of Pathology, Amsterdam UMC, Amsterdam, Netherlands, <sup>4</sup>Department of Gastroenterology and Hepatology, Amsterdam UMC, Amsterdam, Netherlands

Recent literature suggests that tri-exponential models may provide additional information and fit liver intravoxel incoherent motion (IVIM) data more accurately than conventional bi-exponential models. However, voxel-wise fitting of IVIM results in noisy and unreliable parameter maps. For bi-exponential IVIM, neural networks (NN) were able to produce superior parameter maps than conventional least-squares (LSQ) generated images. Hence, to improve parameter map quality of tri-exponential IVIM, we developed an unsupervised physics-informed deep neural network (IVIM<sub>3</sub>-NET). We assessed its performance in simulations and in patients with non-alcoholic fatty liver disease (NAFLD) and compared outcomes with bi-exponential LSQ and NN fits and tri-exponential LSQ fits. Scanning was performed using a 3.0T free-breathing multi-slice diffusion-weighted single-shot echo-planar imaging sequence with 18 b-values. Images were analysed for visual quality, comparing the bi- and tri-exponential IVIM models for LSQ fits and NN fits using parameter-map signal-to-noise ratios (SNR) and adjusted  $R^2$ . IVIM parameters were compared to histological fibrosis, disease activity and steatosis grades. Parameter map quality improved with bi- and tri-exponential

**Abbreviations:** ANCHOR, Amsterdam NAFLD-NASH cohort;  $D$ , diffusion;  $D^*$ , pseudo-diffusion;  $D_1^*$ , slow pseudo-diffusion;  $D_2^*$ , fast pseudo-diffusion;  $f_1$ , slow perfusion fraction;  $f_2$ , fast perfusion fraction; IVIM, intravoxel incoherent motion; IVIM-NET, neural network for bi-exponential IVIM fitting; IVIM<sub>3</sub>-NET, neural network for tri-exponential IVIM fitting; LSQ, least-squares; NAFLD, non-alcoholic fatty liver disease; ROI, region of interest; ROIliver, region of interest of entire liver excluding large vessels; ROISNR, small region of interest in homogenous liver tissue; SENSE, parallel imaging factor; SNR, signal-to-noise ratio; SPAIR, spectral attenuated inversion recovery;  $S_0$ , signal intensity at  $b = 0$ .

NN approaches, with a significant increase in average parameter-map SNR from 3.38 to 5.59 and 2.45 to 4.01 for bi- and tri-exponential LSQ and NN models respectively. In 33 out of 36 patients, the tri-exponential model exhibited higher adjusted  $R^2$  values than the bi-exponential model. Correlating IVIM data to liver histology showed that the bi- and tri-exponential NN outperformed both LSQ models for the majority of IVIM parameters (10 out of 15 significant correlations). Overall, our results support the use of a tri-exponential IVIM model in NAFLD. We show that the IVIM<sub>3</sub>-NET can be used to improve image quality compared to a tri-exponential LSQ fit and provides promising correlations with histopathology similar to the bi-exponential neural network fit, while generating potentially complementary additional parameters.

#### KEYWORDS

magnetic resonance imaging, diffusion magnetic resonance imaging, non-alcoholic fatty liver disease, intravoxel incoherent motion (IVIM), deep learning, tri-exponential, unsupervised learning

## Introduction

The prevalence and degree of obesity and type 2 diabetes mellitus are increasing worldwide, resulting in a concomitant increase in non-alcoholic fatty liver disease (NAFLD), which is now the most prevalent global liver disease (Younossi et al., 2016). NAFLD is characterized by an accumulation of lipids within hepatocytes, known as steatosis, which in turn can trigger intracellular events in the liver, such as hepatocyte ballooning, lobular inflammation and ultimately liver fibrosis (Parthasarathy et al., 2020). NAFLD can lead to liver-related complications such as cirrhosis and hepatocellular carcinoma (Younossi et al., 2016), and is also thought to contribute to an increased risk of atherosclerotic cardiovascular disease (Targher et al., 2016; Stefan et al., 2019). Liver biopsy is currently the gold standard for diagnosing and staging NAFLD, assessing levels of steatosis, inflammation, ballooning and fibrosis from a small tissue sample. Several disadvantages of liver biopsy include patient discomfort, a small, yet severe risk of life-threatening intraperitoneal haemorrhage and inaccuracies due to sampling error (Gilmore et al., 1995; Seeff et al., 2010). This has led to a growing interest in non-invasive techniques for detecting the presence and severity of NAFLD. MRI has been developed and researched as a diagnostic tool in NAFLD (Unal et al., 2017). Various methods have been proposed, of which intravoxel incoherent motion (IVIM) imaging has shown potential as a biomarker for assessing and staging NAFLD, particularly for levels of fibrosis (Li et al., 2017).

IVIM assesses tissue diffusivity and perfusion reflected by random motion of water molecules in the intracellular and extracellular spaces as well as in the tissue (micro)circulation, respectively (Le Bihan et al., 1988). Data acquired using a range of diffusion weightings (b-values) are typically fitted using a bi-exponential model using the following formula:

$$S(b) = S_0 \cdot \left( (1 - f) \cdot e^{-bD} + f \cdot e^{-bD^*} \right) \quad (1)$$

where diffusion ( $D$ ), pseudo-diffusion ( $D^*$ ) and perfusion fraction ( $f$ ) parameters are estimated, with  $S_0$  equating the signal intensity for  $b = 0 \text{ s/mm}^2$ . NAFLD has the potential to alter IVIM parameters in multiple ways. In the case of fibrosis, it can be theorized that the increased collagen depositions in the liver restrict the free movement of water molecules, leading to a reduction in the diffusion parameters, while increased hepatic resistance amongst others can lead to a reduction in hepatic perfusion. Li et al. show that while absolute values tend to vary between studies, typically a decrease in all three IVIM parameters is observed as fibrosis stage increases (Li et al., 2017). Hepatic inflammation could be thought to decrease perfusion parameters in particular due to the inflammatory response, in which cell infiltration and oedema restrict blood flow in the capillaries. Hepatocellular ballooning leads to increases in cell size and therefore in theory could restrict both diffusion and perfusion parameters. While the literature on IVIM for assessing inflammation or ballooning grades is less readily available, the existing literature describes a negative correlation between perfusion fraction and both inflammation and ballooning (Murphy et al., 2015).

Recent literature suggests that the bi-exponential IVIM model may be insufficient for fitting the liver's complex structure. The marked signal decay in the IVIM signal intensity plots seen at low b-values has given rise to the hypothesis that a tri-exponential model will provide a more accurate representation of the data and improve fit accuracy (Chevallier et al., 2021). Herein, an extra exponent is added to improve this fitting of rapid signal decay at very low b-values:

$$S(b) = S_0 \cdot \left( (1 - f_1 - f_2) \cdot e^{-bD} + f_1 \cdot e^{-bD_1^*} + f_2 \cdot e^{-bD_2^*} \right) \quad (2)$$

where diffusion ( $D$ ), slow ( $D_1^*$ ) and fast pseudo-diffusion ( $D_2^*$ ), and slow ( $f_1$ ) and fast perfusion fraction ( $f_2$ ) are estimated. While the origin of the tri-exponential behaviour in the liver is

still being debated, one leading theory is that  $f_1$  signal could arise from slower incoherent sinusoid perfusion, while  $f_2$  signal could originate from rapid dephasing of coherent flow in opposing directions or laminar flow profiles in larger vessels (Riexinger et al., 2020). Available studies advocating the use of a tri-exponential model show a higher goodness of fit when compared to a bi-exponential model (Cercueil et al., 2015; Chevallier et al., 2019; Riexinger et al., 2020), seen by an improved Akaike information criterion amongst others. However, the drive towards tri-exponential models is predominantly based on the fit better describing the data, as the tri-exponential model has only been implemented in healthy volunteers. Whether the added fit parameters have value for disease classification, such as in patients with NAFLD, yet needs to be investigated.

Although tri-exponential fitting more accurately describes the data, fitting of this complex model is challenging and current least-squares (LSQ) methods typically lead to noisy parameter maps, particularly in the case of pseudo-diffusion. As a result, tri-exponential fits are often done using averaged data from a region of interest (ROI), or even averaged data from multiple subjects, instead of voxel-wise fitting, reducing clinical diagnostic applicability.

To improve parameter map accuracy, the use of deep neural networks to model the bi-exponential IVIM fit has been proposed (Bertleff et al., 2017; Barbieri et al., 2020; Kaandorp et al., 2021; Koopman et al., 2021; Lee et al., 2021). In a previous study, a physics-informed unsupervised approach that could train directly to *in-vivo* MRI data (IVIM-NET) (Barbieri et al., 2020; Kaandorp et al., 2021) was implemented. IVIM-NET provided parameter maps that were less noisy, visually more detailed and had a higher test-retest repeatability. However, there is not yet a tri-exponential equivalent to the neural network. This approach could substantially improve the voxel-wise fitting of tri-exponential IVIM, enabling parameter maps with clinically acceptable quality and aid wider spread implementation.

Therefore, in this work, we aim to investigate the value of a deep neural network to fit a tri-exponential model to IVIM data in NAFLD. We split up the research into two sub-questions: firstly, does the parameter map quality improve when introducing neural networks for fitting the bi- and tri-exponential models? Secondly, is there an added value of tri-exponential fitting in the non-invasive grading of NAFLD disease severity? To address these questions, we have developed a deep neural network to fit a tri-exponential model to IVIM data (IVIM<sub>3</sub>-NET). To show our network works, we compared the performance of IVIM<sub>3</sub>-NET to LSQ fitting in simulations. We then tested the tri-exponential versus bi-exponential model in patients with various stages of NAFLD, and compared the use of IVIM-NET and IVIM<sub>3</sub>-NET to conventional bi- and tri-exponential LSQ fits.

## Materials and methods

### Design

Patient data were collected as part of the ongoing Amsterdam NAFLD-NASH cohort (ANCHOR) study as described in previous work (Troelstra et al., 2021). In this previous clinical work, the correlations between liver histopathology and several ultrasonographic and MRI parameters, including the bi-exponential IVIM-model, were studied. In our current technical work, we use the data to study the tri-exponential model and the performance of NNs. All patients underwent an MRI scan of the liver and ultrasound-guided liver biopsy, amongst other diagnostic tests. The study was conducted at Amsterdam University Medical Centre, in compliance with the principles in the declaration of Helsinki and according to Good Clinical Practice guidelines. The protocol was reviewed and approved by the institutional review board of the AMC and was registered in the Dutch Trial Register (registration number NTR7191). All participants provided written informed consent before study activities.

### Participants

36 individuals with known hepatic steatosis (confirmed on ultrasound), a BMI >25 kg/m<sup>2</sup> and elevated aspartate aminotransferase and/or alanine aminotransferase levels were included. The main exclusion criteria were contraindications for undergoing MRI, any condition or risk factors potentially leading to liver disease besides NAFLD (excessive alcohol use, drug-use, hepatitis, etc.), conditions or risk factors leading to bleeding disorders and decompensated liver cirrhosis or hepatocellular carcinomas. Participants were required to fast for a minimum of 4 h before diagnostic tests.

### MRI acquisition

MRI scanning was performed using a 3.0T MRI scanner (Ingenia; Philips, Best, Netherlands) with a 16-channel phased-array anterior coil and 10-channel phase-arrayed posterior coil. IVIM data were acquired using a free-breathing multi-slice diffusion-weighted single-shot echo-planar imaging sequence. Eighteen unique b-values were acquired: 0, 1, 2, 5, 10, 20, 30, 40, 50, 75, 100, 150, 200, 300, 400, 500, 600, and 700 s/mm<sup>2</sup> in three orthogonal directions. The following acquisition parameters were used: repetition time 7,000 ms, echo time 45.5 ms, bandwidth 20.8 Hz/pixel in phase encoding direction, field-of-view 450 × 295 mm<sup>2</sup> with a 3.0 × 3.0 mm<sup>2</sup> acquisition resolution, 152 × 97 acquisition matrix, 27 slices with a 6.0 mm slice thickness and 1.0 mm slice gap, parallel imaging factor (SENSE) 1.3, partial averaging factor 0.6, spectral attenuated

inversion recovery (SPAIR) fat suppression and three saturation slabs to suppress signal from the anterior abdominal wall. The total acquisition time was 8.1 min.

## MRI analysis

Images were analysed by a single observer (M.T.) with 4 years of experience in hepatic MRI. The entire liver was manually segmented using reconstructed b-value = 0 images, avoiding liver edges and any areas or slices containing (motion) artefacts (ROI<sub>liver</sub>). Four different models were used to fit the ROI<sub>liver</sub>, all implemented in Python (version 3.6.12). These consisted of our newly developed IVIM<sub>3</sub>-NET tri-exponential fit, the IVIM-NET bi-exponential fit, and the LSQ bi- and tri-exponential fits. Data were normalized to the  $S(b = 0 \text{ s/mm}^2)$  for all fitting methods. For the deep learning approaches, we used PyTorch (1.8.1) whereas the least-squares fitting was done with scipy's (1.5.2) optimize.curve\_fit function. All fitting methods can be found on <https://github.com/oliverchampion/IVIMNET> (commit 751f272 on 14 Dec 2021).

## Bi- and tri-exponential LSQ fits

The LSQ models were fit voxel-wise, solving the bi- or tri-exponential model for all segmented voxels. For the bi-exponential LSQ fitting, Eq. 1 was fitted directly, with fit

constraints  $3 \times 10^{-4} < D < 5 \times 10^{-3} \text{ mm}^2/\text{s}$ ,  $0 < f < 0.7$ ,  $5 \times 10^{-3} < D^* < 3 \times 10^{-1} \text{ mm}^2/\text{s}$  and  $0.5 < S_0 < 2.5 \text{ mm}^2/\text{s}$ . For the tri-exponential LSQ fitting, Eq. 2 was modified and we fitted:

$$S(b) = f'_0 \cdot e^{-b \cdot D} + f'_1 \cdot e^{-b \cdot D_1^*} + f'_2 \cdot e^{-b \cdot D_2^*} \quad (3)$$

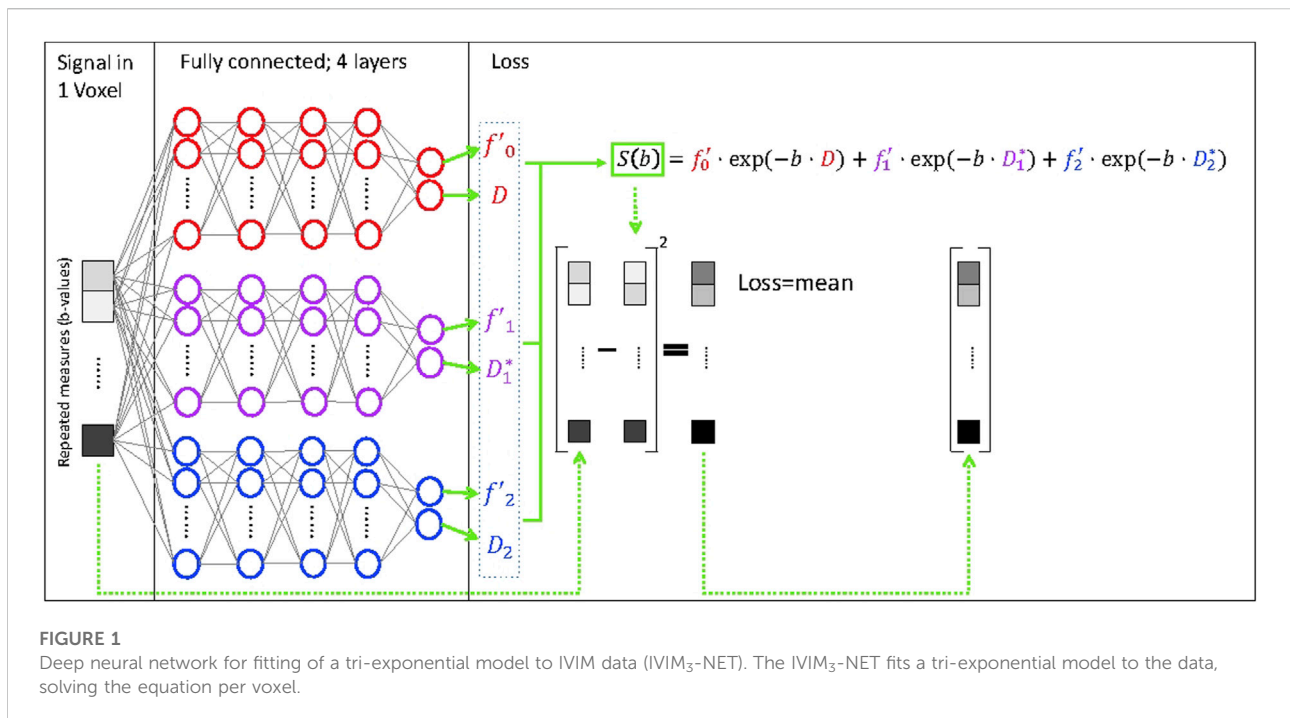
with  $S_0 = f'_0 + f'_1 + f'_2$ ,  $f_1 = f'_1/S_0$ ; and  $f_2 = f'_2/S_0$ .

Constraints were implemented ensuring  $0 < D < 8 \times 10^{-3} \text{ mm}^2/\text{s}$ ,  $8 \times 10^{-3} < D_1^* < 80 \times 10^{-3} \text{ mm}^2/\text{s}$ ,  $60 \times 10^{-3} < D_2^* < 5 \text{ mm}^2/\text{s}$ ,  $0 < f'_0 < 2.5$ ,  $0 < f'_1 < 1$  and  $0 < f'_2 < 1 \text{ mm}^2/\text{s}$ . The  $f_1$  and  $f_2$  of the tri-exponential model were also summed to produce a  $f_{1+2}$  parameter map for direct comparison with the perfusion fraction  $f$  of the bi-exponential model.

To determine goodness of fit, the bi- and tri-exponential LSQ models were also separately fit in a ROI-wise manner using the ROI<sub>liver</sub>. Here the average value per individual and per b-value was fit using the same constraints as described above, increasing the signal-to-noise ratio (SNR). Fitting was done in a parallel routine, using eight cores from an Intel(R) Xeon(R) Gold 6132 CPU at 2.60 GHz and fitting times were recorded.

## IVIM-NET and IVIM<sub>3</sub>-NET fits

IVIM-NET bi and tri-exponential fits were also performed voxel-wise. The IVIM-NET bi-exponential fit was performed following previously published work, using a fully-connected network per IVIM parameter ( $S_0$ ,  $D$ ,  $D^*$  and  $f$ ) and a physics-informed loss function to minimize the root-mean-square error



between input voxel signals and predicted signal decay. The hyperparameters were kept identical to the optimized setting previously published (Kaandorp et al., 2021), with a dropout of 0.1, batch normalization, two hidden layers, Adam optimizer and a learning rate of  $3 \times 10^{-5}$ .

The tri-exponential IVIM<sub>3</sub>-NET was developed based on the IVIM-NET, adapting the physics-informed loss function to a tri-exponential model (Eq. 3, Figure 1), instead of the previously reported bi-exponential model. As the tri-exponential model is more challenging to fit than the bi-exponential model, we made some additional adaptations to the network. We introduced a semi-parallel training approach, which was a variation on the parallel training from IVIM-NET. Instead of having each parameter estimated by a separate network, however, each pair of decay constants and signal fractions ( $f'_0$  with  $D$ ;  $f'_1$  and  $D_1^*$ ;  $f'_2$  and  $D_2^*$ ) were predicted by a network. We used four hidden layers (instead of 2). We also started at a higher learning rate of  $1 \times 10^{-4}$  and introduced a scheduler that decreased the learning rate by a factor of five each time the network did not improve performance on the validation data for 10 consecutive iterations. Early stopping was then adapted such that once the performance did not decrease in the initial 10 iterations of a new learning rate, training was stopped.

Both networks were trained on the *in vivo* liver data from all 36 patients, resulting in 3,304,437 voxels. Data were split into 90% for training and 10% for testing. As data was trained unaware of the ground truth, we could use the same networks for predicting the parameter maps (Kaandorp et al., 2021). Note that each epoch <2% of data is seen and that training is completed in median 91 epochs, meaning each data point is seen less than twice. Training and inference were done on a Tesla P100 GPU and times were recorded (averaged over 10 repeated training/inference).

## Comparison of image quality tri-exponential fits

All tri-exponential LSQ and NN images were assessed by a single observer (M.T.) in a side-by-side fashion. Image preference was recorded per slice per patient based on subjective image quality analysis.

## Simulated data

Simulations run in previous work for the bi-exponential IVIM-NET showed that the neural network approach resulted in a smaller error compared to other methods, particularly when compared to the LSQ fit (Barbieri et al., 2020; Kaandorp et al., 2021). To confirm that this also applied to the IVIM<sub>3</sub>-NET tri-exponential approach, we ran simulations and determined the root mean square error

between the predicted parameters and the ground truth parameters used to simulate the data. To train the network, 5,000,000 signal curves were simulated at the same b-values acquired *in vivo*, using randomly selected IVIM parameters ranging from  $0.5 \times 10^{-3} \text{ mm}^2/\text{s} > D > 3 \times 10^{-3} \text{ mm}^2/\text{s}$ ,  $0.05 > f > 0.3$ ,  $10 \times 10^{-3} \text{ mm}^2/\text{s} > D_1 > 50 \times 10^{-3} \text{ mm}^2/\text{s}$ ,  $0.05 > f_2 > 0.3$  and  $0.2 \text{ mm}^2/\text{s} > D_2 > 4 \text{ mm}^2/\text{s}$ . These boundaries were representative for values found *in vivo*. Random Gaussian noise was added with SNR exponentially distributed between 10 and 100. From preliminary results, we found there were two local minima for training, and three out of 10 networks ended up in a poorly performing local minima, with loss substantially higher than the other 7. Therefore, training was repeated 10-fold and the network with the lowest unsupervised training loss was used for further analysis. Four new datasets were created for testing, each consisting of 300,000 randomly generated tri-exponential IVIM curves from similarly distributed parameter values. Each dataset had a different SNR, namely, 15, 20, 30 and 50. Both the trained IVIM<sub>3</sub>-NET and LSQ fit were performed on these new datasets and the root-mean-square errors (RMSE) between their predicted values and the ground truth values were taken as measures for performance.

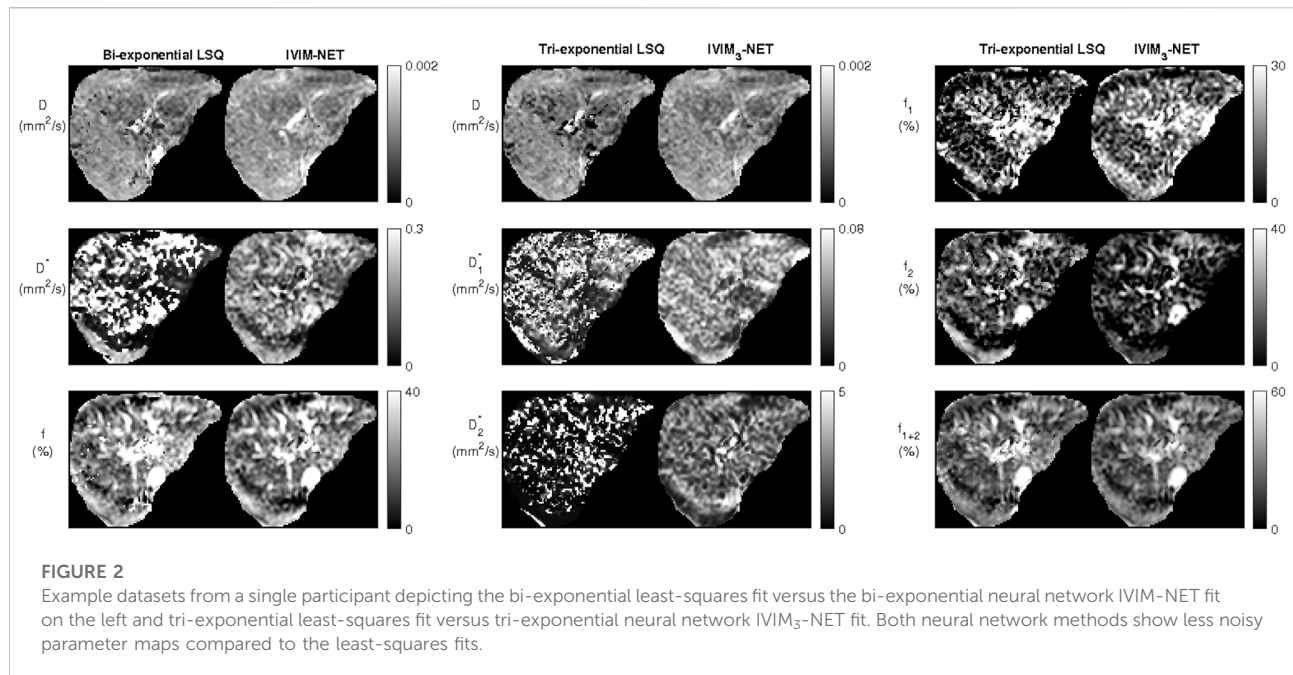
## Liver biopsy

Percutaneous ultrasound-guided liver biopsies acquired after MRI scanning were assessed by an experienced liver pathologist (J.V.). Biopsy length and biopsy quality assessment discerning poor quality, suboptimal quality and good quality were recorded for each sample. Histology specimens were scored according to the steatosis, activity and fibrosis score (Bedossa and FLIP Pathology Consortium, 2014). Steatosis levels were scored accordingly for grades S0-S3. NAFLD disease activity comprised the combined sum of inflammation grade (0–2) and ballooning grade (0–2), for a combined score ranging from grade A0-A4. Fibrosis was scored according to the NASH Clinical Research Network for severity ranging from grades F0-F4 (Kleiner et al., 2005).

## Statistical analysis

The statistical analysis was performed using R version 3.6.3 (R Core Team, 2020).

The SNR of the parameter maps within homogeneous liver tissue was used to determine whether the NN fitting approach was less noisy than the LSQ approach. A separate ROI (ROI<sub>SNR</sub>) was selected in the right liver lobe in homogenous liver tissue, avoiding liver edges, (motion) artefacts and visible vessels. For each individual, the SNR was defined as the ratio of the mean parameter value within ROI<sub>SNR</sub> and the standard deviation from this same ROI<sub>SNR</sub>. Differences between means and SNRs of the



bi- and tri-exponential models were assessed using Wilcoxon signed-rank tests. A  $p$ -value  $< 0.05$  was considered statistically significant.

To determine whether the bi- or tri-exponential model more accurately described the data, we determined the adjusted  $R^2$  of the least-squares fit of the models. As the bi- and tri-exponential models have a different degrees of freedom, we used the adjusted  $R^2$  which corrects for the extra degrees of freedom. As the noise was dominating the voxel-wise adjusted  $R^2$ , we opted for an ROI-wise fit from the ROI<sub>liver</sub>, finding the adjusted  $R^2$  for each individual. Differences between the  $R^2$  of bi- and tri-exponential models were tested using a paired Student t-test. A  $p$ -value  $< 0.05$  was considered statistically significant.

Comparison of histology and the average IVIM parameter values from the ROI<sub>liver</sub> were performed using Spearman's rank correlation for all four models. IVIM<sub>3</sub>-NET parameters were further assessed using Kruskal-Wallis tests for trends, and where appropriate followed by Dunn's post-hoc analysis with  $p$ -value adjustment according to the Holm-Bonferroni method. A  $p$ -value  $< 0.05$  was considered statistically significant.

## Results

### Patient characteristics

The first thirty-six individuals (22 male, 14 female) included in the ANCHOR study were analysed in this work. The average liver biopsy length was 1.81 cm (SD = 0.55). 20 biopsy specimens were classified as good quality, 11 as suboptimal quality and two

poor quality. Quality assessment was not available for three patients included. Liver fibrosis was found on biopsy in all but two patients (F0). Seven patients were classified as F1, nineteen as F2, seven as F3 and one as F4. All patients showed a steatosis level  $\geq 1$  on biopsy, of which 20 patients had S1, twelve S2 and four S3. Three patients had a disease activity grade of A0, twelve A1, fifteen A2, five A3 and one A4.

### Image quality

Visual assessment of IVIM parameter maps revealed that both the neural network methods showed an increased image quality and improved fit accuracy compared to the LSQ methods (Figure 2). For the tri-exponential fit, of the 672 images including liver tissue, the NN showed a higher subjective image quality in 637 slices for  $D$ , 655 slices for  $f_1$ , 636 slices for  $f_2$  and all slices for  $D_1^*$  and  $D_2^*$ . The remaining slices showed comparable image quality, no slices showed superior image quality for the LSQ fit compared to the NN fit. The tri-exponential fit successfully provided parameter maps for all IVIM parameters, with a distinct difference between the  $D_1^*$  and  $D_2^*$  parameters as well as between  $f_1$  and  $f_2$ . Peripheral vessels and liver tissue (e.g. capillaries) showed high  $D_1^*$  and  $f_1$  signals, while  $D_2^*$  and  $f_2$  signals were high in larger vessels. In cases with a lower quality of acquired data, the IVIM<sub>3</sub>-NET was able to provide smoother parameter maps with less extreme outliers than the LSQ fit (Figure 3). Figure 4 displays IVIM<sub>3</sub>-NET parameter maps for three patients with increasing fibrosis grades. While all parameters except  $D_2^*$  show a decrease in signal with increasing fibrosis grade, this effect

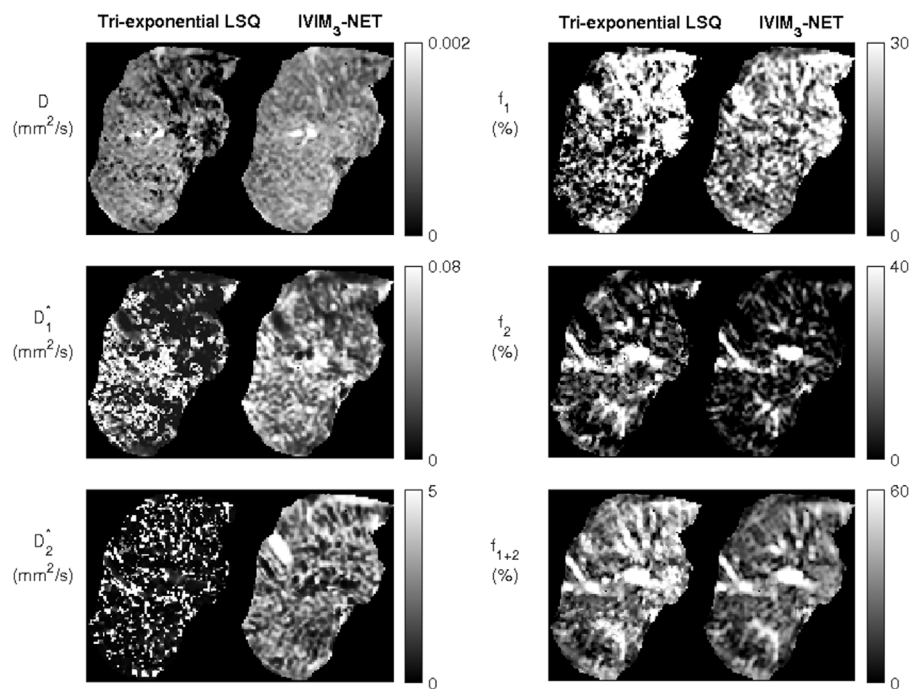


**FIGURE 3**

Example of a noisy dataset from a single participant with lower quality of image acquisition, fit with the tri-exponential least-squares fit and the tri-exponential neural network IVIM<sub>3</sub>-NET. The IVIM<sub>3</sub>-NET provides less noisy parameter maps.

is most noticeable for the perfusion parameter maps ( $f_1$ ,  $f_2$  and  $f_{1+2}$ ).

One patient showed two incidental findings in the liver (Figure 5). Compared to the tri-exponential LSQ fit, the IVIM<sub>3</sub>-NET provided a more distinct delineation of the abnormalities. Interestingly, the two findings displayed different behaviour. The large lesion was most clearly visible on the IVIM<sub>3</sub>-NET pseudo-diffusion maps, with a low  $D_1^*$  signal and a high  $D_2^*$  signal. On the other hand, the small lesion was clearer on the perfusion maps, with a low  $f_1$  signal in and a high  $f_2$  signal.

## Comparison of neural network versus least-squares model

### Simulations

The RMSE of the tri-exponential fits in simulated data with varying SNRs showed a substantially lower error for the IVIM<sub>3</sub>-NET than for LSQ fitting for all parameters and at all tested SNRs (Figure 6). This was particularly evident at lower SNRs, where the largest discrepancies are visible.

### In vivo

The neural network approaches resulted in substantially less noisy, and hence more precise, parameter maps. The average

spread in IVIM values from the ROI<sub>SNR</sub> in homogenous liver tissue showed significantly higher SNRs in the parameter maps for both neural networks fits compared to the LSQ fits for all parameters except the tri-exponential  $f_2$  (Table 1 and Supplementary Figure S1). The average SNR over all parameters was 3.38 versus 5.59 for the bi-exponential LSQ and NN fit respectively and 2.45 versus 4.01 for the tri-exponential LSQ and NN fit respectively.

For the bi-exponential approach, the network took a median of 8.7 min to train, with a range of 6.5–12.8 min, and 40 s to inference ( $1.2 \times 10^{-5}$  s per voxel). For the tri-exponential approach, the network took a median of 12.2 min to train, with a range of 3.4–16.2 min, and 52 s to inference ( $1.5 \times 10^{-5}$  s per voxel). The least-squares fits took substantially longer, with 85 min ( $150 \times 10^{-5}$  s per voxel) for bi-exponential fitting and 166 min ( $300 \times 10^{-5}$  s per voxel) for tri-exponential fitting. Training took a median of 91 epochs before converging.

## Comparison of bi-versus tri-exponential model

The average adjusted  $R^2$  of the LSQ tri-exponential fit for the ROI<sub>liver</sub> was 0.990 for the tri-exponential model and 0.984 for the

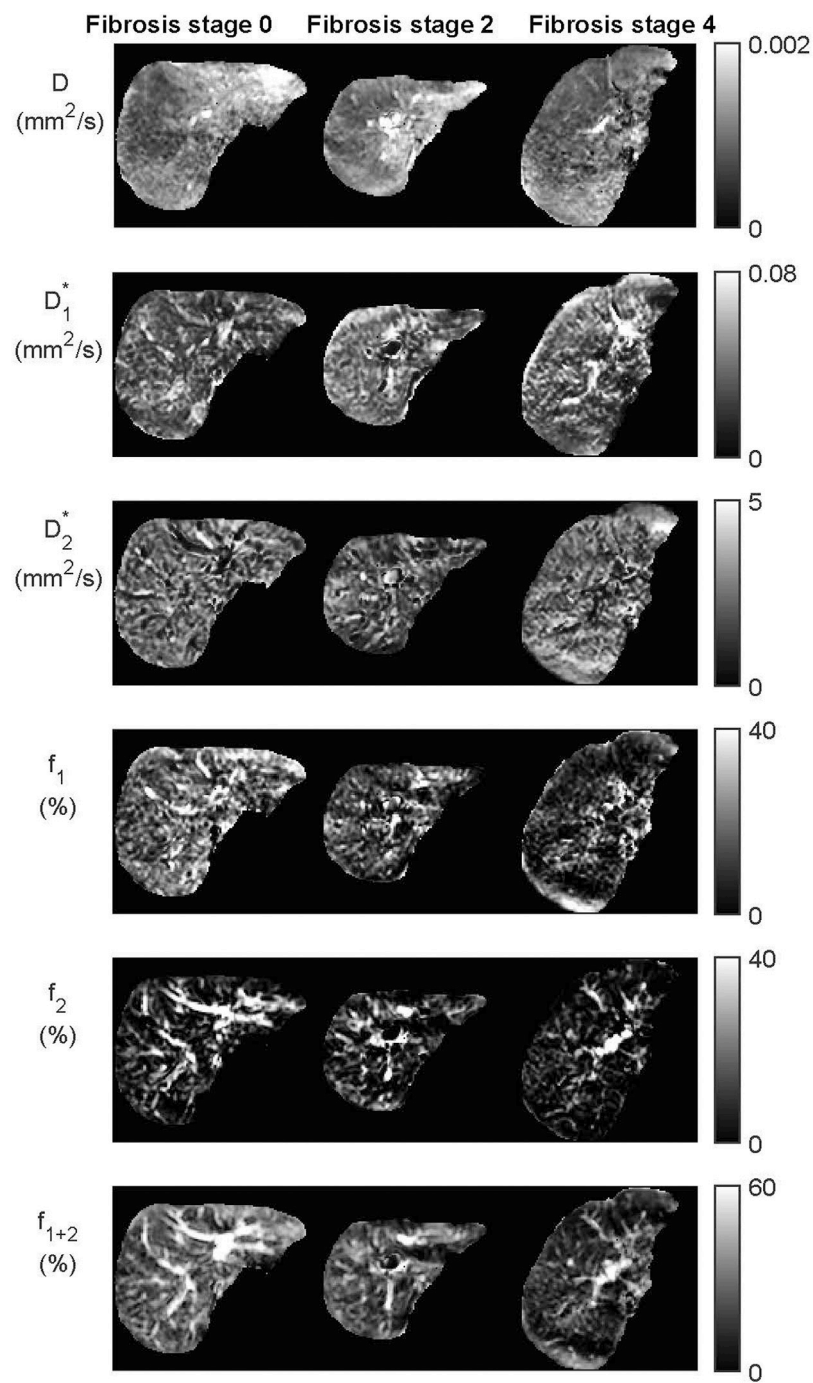


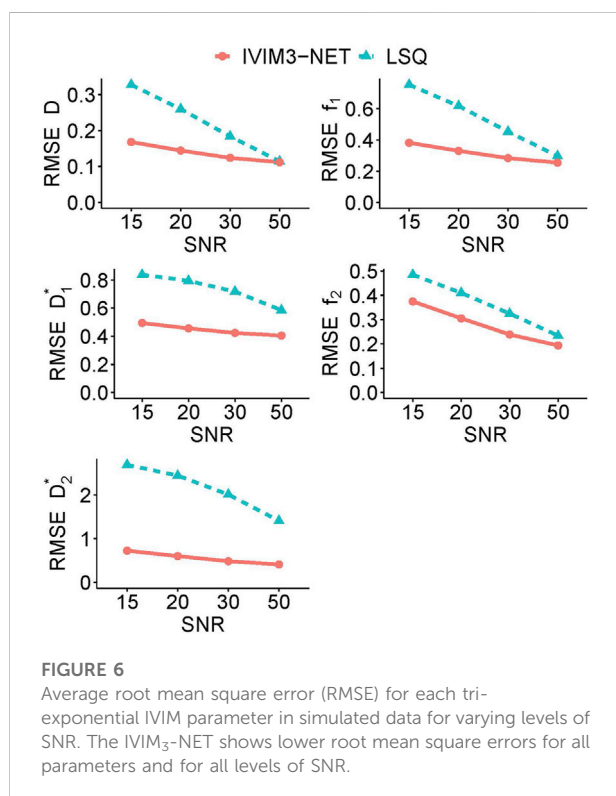
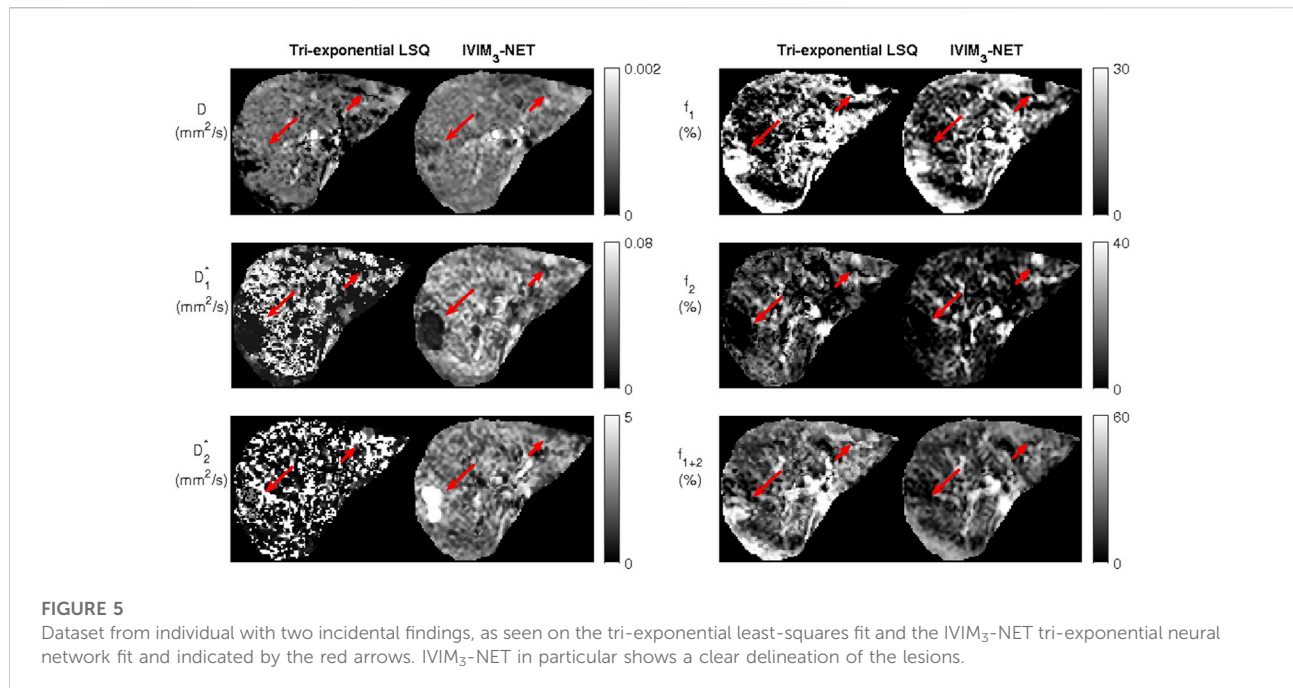
**FIGURE 4**

Datasets from the IVIM<sub>3</sub>-NET tri-exponential neural network of three patients with increasing levels of fibrosis. Visually a decrease of signal intensity with increasing fibrosis stage is most noticeable for the perfusion fractions ( $f_1$ ,  $f_2$  and  $f_{1+2}$ ). Only two patients had fibrosis stage 0 and a single patient fibrosis stage 4.

bi-exponential model ( $t = 6.77$ ,  $df = 35$ ,  $p < 0.001$ ), with a higher adjusted  $R^2$  for the tri-exponential model in 33 out of 36 patients. The bi-exponential and tri-exponential  $R^2$  values of each

individual along with example fits of the best and worst performing tri-exponential fit compared to bi-exponential fit can be found in [Figure 7](#).





## Correlations with liver histopathology

Figure 8 gives an overview of the Spearman correlations between IVIM parameters and histopathology for all the reported

fit methods. Comparing LSQ fits (top two rows) with NN fits (bottom two rows), ten correlations are stronger for the NN than LSQ fit, whereas the LSQ finds five that are stronger than the NN. When comparing bi-exponential to tri-exponential models (using bi-exponential  $f$  and tri-exponential  $f_{1+2}$ ), marginal differences between the four models were found.  $D$  showed higher correlations between histopathology for the bi-exponential model, in particular for the LSQ model. On the other hand,  $f$  was higher for the tri-exponential LSQ model compared to the bi-exponential model, while the NNs showed overall similar values.

## IVIM<sub>3</sub>-NET versus liver fibrosis

IVIM<sub>3</sub>-NET showed a significant decrease in  $D$  ( $r_s = -0.43$ ,  $p = 0.0097$ ),  $f_1$  ( $r_s = -0.47$ ,  $p = 0.0036$ ),  $f_2$  ( $r_s = -0.55$ ,  $p < 0.001$ ) and  $f_{1+2}$  ( $r_s = -0.59$ ,  $p < 0.001$ ) with increasing fibrosis stage.  $D_2^*$  was positively correlated with fibrosis stage ( $r_s = 0.36$ ,  $p = 0.033$ ). Significant differences in medians between fibrosis stages were seen for  $f_1$  ( $\chi^2 = 11.18$ ,  $p = 0.025$ ,  $df = 4$ ),  $f_2$  ( $\chi^2 = 11.00$ ,  $p = 0.027$ ,  $df = 4$ ) and  $f_{1+2}$  ( $\chi^2 = 14.43$ ,  $p = 0.0060$ ), while post-hoc analysis only showed a significant difference between fibrosis stage 0–3 for  $f_1$  and  $f_{1+2}$  (Figure 9).

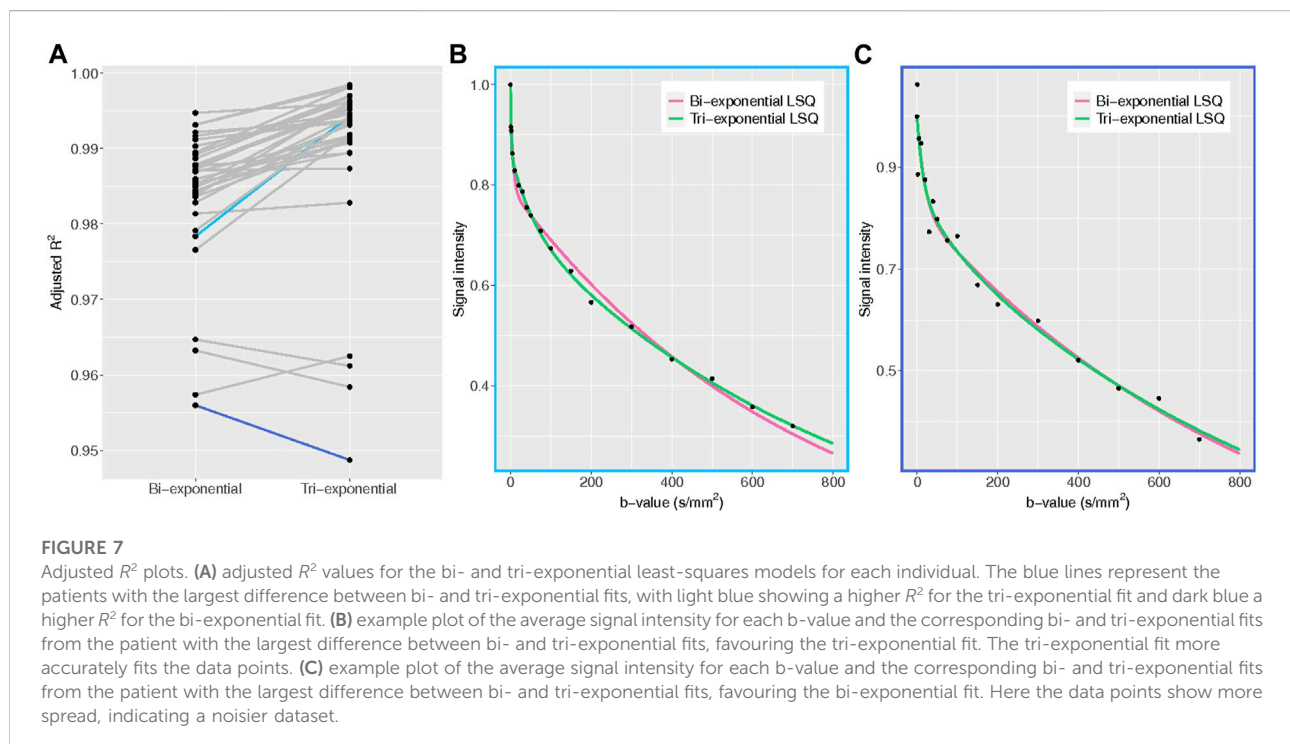
## IVIM<sub>3</sub>-NET versus NASH disease activity

A significant correlation was observed between disease activity grade and all IVIM<sub>3</sub>-NET parameters except  $D_1^*$  ( $D$ :  $r_s = -0.35$ ,  $p = 0.040$ ;  $D_2^*$ :  $r_s = 0.42$ ,  $p = 0.011$ ;  $f_1$ :  $r_s = -0.36$ ,  $p = 0.029$ ;  $f_2$ :  $r_s = -0.49$ ,  $p = 0.0024$ ;  $f_{1+2}$ :  $r_s = -0.48$ ,  $p = 0.0029$ ) was observed, with  $f_2$  and  $f_{1+2}$  showing significant differences between disease activity grades ( $\chi^2 = 9.77$ ,  $p = 0.044$ ,  $df = 4$ ;  $\chi^2 = 9.97$ ,  $p = 0.041$ ,  $df = 4$  respectively). Post-hoc analysis,

**TABLE 1** Mean parameter values from the entire liver excluding large vessels ( $ROI_{liver}$ ) and mean signal-to-noise ratio (SNR) from the small region-of-interest in homogenous liver tissue ( $ROI_{SNR}$ ) for all four IVIM models per IVIM parameter.

	Bi-exponential LSQ		Bi-exponential NN		Tri-exponential LSQ		Tri-exponential NN	
	Mean	SNR	Mean	SNR	Mean	SNR	Mean	SNR
$D$ (10–3 mm <sup>2</sup> /s)	1.02	5.47	1.24	9.33***	0.94	5.53	1.12	8.26***
$D_1^*$ (mm <sup>2</sup> /s)	0.12	1.38	0.15	3.79***	0.032	1.80	0.042	4.65***
$D_2^*$ (mm <sup>2</sup> /s)					1.49	0.83	2.27	4.10***
$f_1$ (%)					15.89	1.50	15.80	2.26***
$f_2$ (%)					13.31	1.83***	8.35	1.18
$f_{1+2}$ (%)	26.28	3.30	19.91	3.66*	29.20	3.23	24.15	15 3.60**

The bi-exponential neural network (NN) model had significantly higher means for the  $D$  and  $D^*$  parameters, while the  $f$  was higher for bi-exponential least-squares (LSQ) model. The SNR was higher for all bi-exponential NN parameters. The tri-exponential NN model had a higher mean values for the  $D$ ,  $D_1^*$  and  $D_2^*$  parameters; the tri-exponential LSQ model had higher means for the  $f_1$ ,  $f_2$  and  $f_{1+2}$  parameters. SNR of the tri-exponential NN model was significantly higher than the tri-exponential LSQ model for all parameters except  $f_2$  (LSQ higher than NN) and  $f_{1+2}$  (no significant difference between NN and LSQ). \*: significantly higher SNR than other bi- or tri-exponential model with  $0.01 < p\text{-value} < 0.05$ . \*\*: significantly higher SNR than other bi- or tri-exponential model with  $0.001 < p\text{-value} < 0.01$ . \*\*\*: significantly higher SNR than other bi- or tri-exponential model with  $p\text{-value} < 0.001$ . LSQ: least-squares, NN, neural network, SNR, signal-to-noise ratio.



however, did not provide significant differences between individual disease activity grades (Figure 10).

### IVIM<sub>3</sub>-NET versus hepatic steatosis

Steatosis grade did not correlate with any IVIM<sub>3</sub>-NET parameter and no significant differences between group medians were found (Supplementary Figure S2).

## Discussion

Our IVIM<sub>3</sub>-NET is the first neural network able to provide high-quality tri-exponential IVIM parameter maps and IVIM<sub>3</sub>-NET is shared on our GitHub. We had four main findings: first, IVIM<sub>3</sub>-NET provides substantially more precise parameter estimates. This was confirmed in simulations, where the

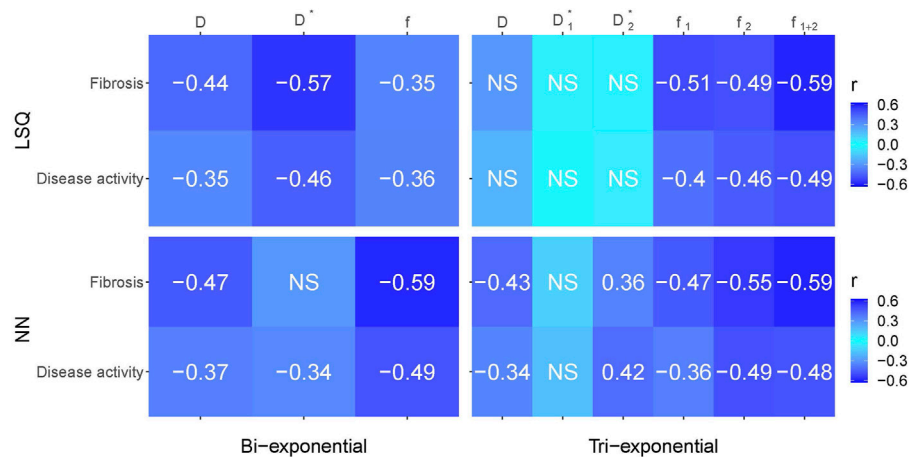


FIGURE 8

Spearman correlations between histopathological outcomes fibrosis and disease activity versus IVIM parameters for the bi- and tri-exponential least-squares methods (LSQ) and the bi- and tri-exponential neural network methods (NN). Darker blue equates a stronger negative or positive correlation. Only significant values ( $p < 0.05$ ) are reported, non-significant values are depicted by NS.

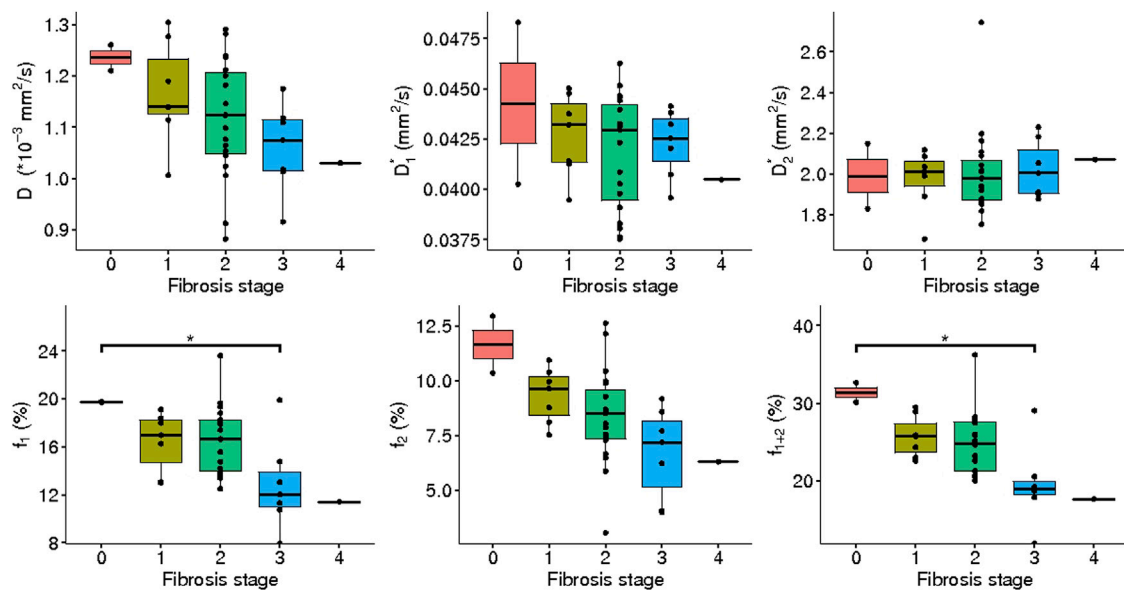
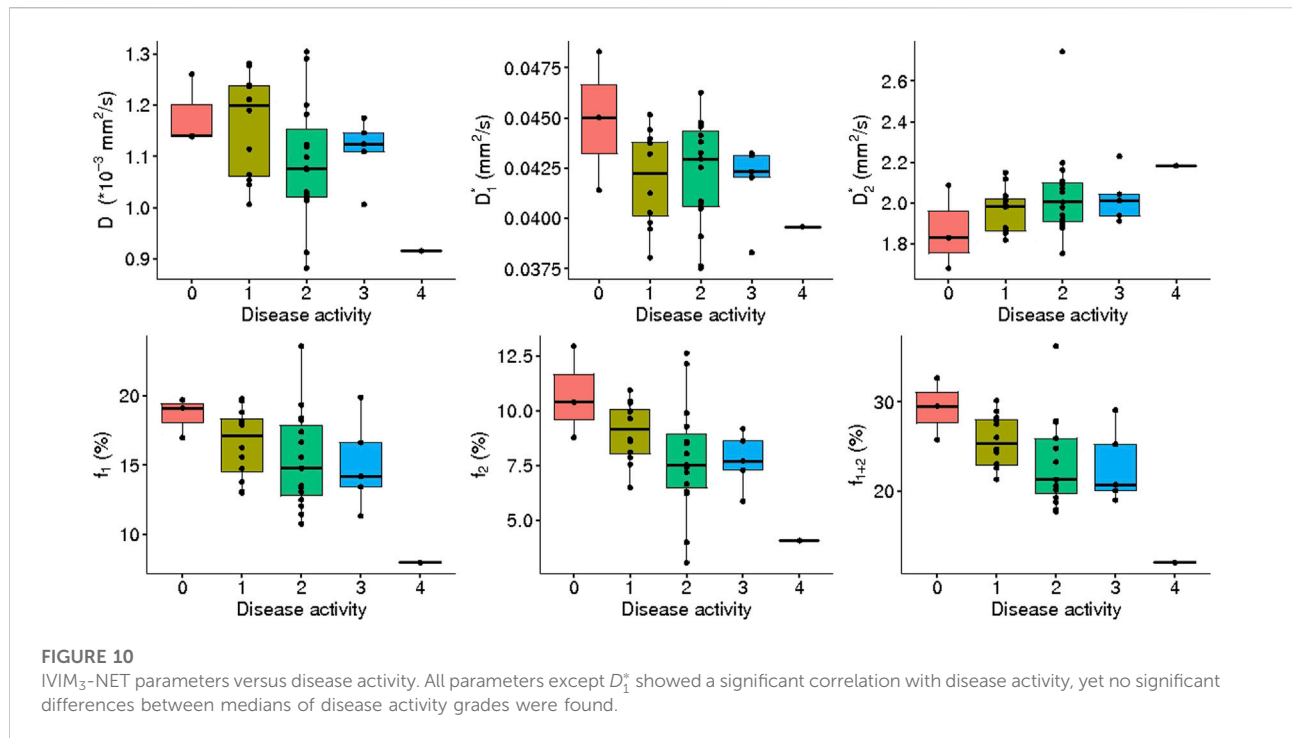


FIGURE 9

IVIM<sub>3</sub>-NET parameters versus fibrosis grade. All parameters except  $D_1^*$  showed a significant correlation with fibrosis, while only  $f_1$  showed a significant difference in medians between fibrosis stage 0 and 3;  $f_{1+2}$  between stage 0 and 3, as well as stage 1 and 3.

RMSE was considerably lower for the IVIM<sub>3</sub>-NET than LSQ fits for all parameters and at all SNRs. The better estimates resulted in improved parameter map quality, as both neural networks provided a less noisy fit than the LSQ fits. Second, the neural network was substantially faster and produced parameter maps in times that would allow for immediate on-console evaluation. Third, the majority of patients with NAFLD displayed a

significantly higher adjusted  $R^2$  for the tri-exponential model compared to the bi-exponential model, suggesting that the data behaves in a tri-exponential manner and hence should be fitted by a tri-exponential model. However, we did not find a clear clinical advantage of the tri-exponential model parameters compared to the bi-exponential model parameters in our cohort. Fourth, correlating IVIM data to liver histology results



**FIGURE 10**

IVIM<sub>3</sub>-NET parameters versus disease activity. All parameters except  $D_1^*$  showed a significant correlation with disease activity, yet no significant differences between medians of disease activity grades were found.

from patients with varying levels of NAFLD severity showed that both the IVIM<sub>3</sub>-NET and IVIM-NET showed similar diagnostic performance, while generally outperforming both the bi- and tri-exponential least-squares models.

Multiple studies in healthy volunteers support the use of a tri-exponential model for assessing IVIM scans of the liver. For example, Cercueil et al. (2015), RieXinger et al. (2019) and Chevallier et al. (2019) all assessed the use of a tri-exponential model of the liver compared to a bi-exponential model and showed an improvement in the Akaike information criterion for the tri-exponential model amongst others. To our knowledge, we are the first to assess the use of a tri-exponential model with an extra fast diffusion component in patients with liver disease. Our results also support the use of a tri-exponential model, seen by a higher adjusted  $R^2$  in the majority of subjects.

The clinical added value of the extra compartment is less clear in our cohort, as both the bi- and tri-exponential models showed comparable correlations with histopathology. However, NAFLD is known to cause vascular changes (Pasarín et al., 2017), thus particularly the evaluation of the additional perfusion parameter  $f_2$  could be of interest, as this signal originates from larger vessels (Chevallier et al., 2021). We (visually) observed a large decrease in  $f_2$  volumes with increasing levels of fibrosis (Figure 4), which could lead to radiological markers for disease severity.

While our cohort contained the full spectrum of NAFLD disease severity, only a single patient had fibrosis stage 4 and two with fibrosis grade 0. Similarly, for disease activity, only a single patient exhibited grade A4. This is a large limitation of the

current study and future studies with larger cohorts with more patients in the higher and lower ranges of disease severity will be required to confirm the results and potentially improve disease severity stratification.

The use of a neural network for the generation of IVIM parameter maps resulted in higher quality images when compared to a least-squares fit, and in a fraction of the time. Simulated data shows a smaller error for the IVIM<sub>3</sub>-NET than LSQ fit, in particular at lower SNRs, confirming the results seen for the bi-exponential IVIM-NET (Kaandorp et al., 2021). A higher correlation was found between histopathology and neural network IVIM parameters compared to LSQ fits, highlighting a promising application for the use of the IVIM-NET and IVIM<sub>3</sub>-NET parameters as a non-invasive biomarker in NAFLD. Moreover, with the improved image quality, additional information may be available. Improved image quality allows for the analysis of images in a voxel-wise manner and may be able to provide more insights into disease pathophysiology. The visual decrease of areas with high signal intensity on  $f_1$  and  $f_2$  images with increasing fibrosis grades may, for example, be indicative of the before mentioned vascular changes in NAFLD. Thus voxel-wise assessment of images, such as volume of voxels with higher signal intensities, could be an interesting route to explore. Furthermore, while IVIM studies tend to focus on quantitative measures, improved parameter map quality may allow for qualitative assessment of images, for example aiding diagnosis of liver lesions such as presented in Figure 5.

For healthy volunteers, an overview of average tri-exponential IVIM-values was published in a recent review (Chevallier et al., 2021). Values for  $D$  ranged between

0.98–1.35  $\times 10^{-3}$  mm<sup>2</sup>/s which is in line with what we found with the IVIM<sub>3</sub>-NET and higher than our tri-exponential LSQ fit as seen in **Table 1**.  $D_1^*$  values were similar to values found in our patient cohort, with reported values ranging between 15.4 and 81.3  $\times 10^{-3}$  mm<sup>2</sup>/s. The largest variation was found in the  $D_2^*$  parameter, with values between 270 and 2,453  $\times 10^{-3}$  mm<sup>2</sup>/s. The  $D_2^*$  values of both tri-exponential models in our study fit fall in this range, however, the IVIM<sub>3</sub>-NET values were at the high end of the range. The  $f_1$  values of both methods fell within the reported range of 7.8–17.6%, while  $f_2$  was lower than reported values of 10.8–17.1 for the IVIM<sub>3</sub>-NET only.

Discrepancies between values found in this study and previous studies could in part be explained by intrinsic effects caused by NAFLD. We would expect the values in the literature derived from healthy volunteers to be most comparable to patients exhibiting a lesser NAFLD severity, i.e. low levels of fibrosis and disease activity. From **Figures 9, 10** it is clear that  $D_2^*$  increases with disease activity and fibrosis stage and other parameters including  $f_2$  decrease, suggesting that healthy volunteers could have a lower  $D_2^*$  and higher  $D$ ,  $D_1^*$ ,  $f_1$  and  $f_2$  than we find in our population.

The wide spread in  $D_2^*$  could in part be due to the b-value distribution. Riexinger et al. investigated the effects of the number of b-values acquired, showing that in particular  $D_2^*$  was highly influenced by the number of low b-values due to an increase in fit accuracy, with an increase in  $D_2^*$  as the number of b-values is increased (Riexinger et al., 2020). The b-value distribution used in this study was optimized for a bi-exponential model and included fewer low b-values than the recommended five to eight b-values < 6 s/mm<sup>2</sup>. Despite this, our IVIM<sub>3</sub>-NET showed  $D_2^*$  values in the high end of the range of previously published work. This could in part be explained by the fact that the IVIM<sub>3</sub>-NET is relatively uninfluenced by the presence of noise compared to the LSQ fit. Comparison of other optimisation techniques such as free-breathing acquisitions versus respiratory or navigator triggering, as well as motion correction methods are not yet available for tri-exponential fitting and are likely to influence absolute parameter values. In future work these effects will need to be further assessed to optimise and standardize scan protocols.

Bayesian fitting techniques resulted in comparable parameter map quality to the IVIM-NET for bi-exponential fitting, however, are impractical for tri-exponential fitting due to long calculation times (Kaandorp et al., 2021). Setting tighter fit constraints for the least-squares model may result in less noisy parameter maps. However, the same is true for the neural network, which had identical constraints in this work. Our chosen fit constraints were relatively broad to encompass an expected large spread in values between participants, but further work will be required to determine the optimal settings in this population. Finally, denoising the DWI data (Manjón et al., 2013; Gurney-Champion et al., 2019) as a pre-processing step may reduce the noise in the parameter maps of the least-squares fit. However, we opted against denoising as it often introduces

blurring of images. Furthermore, denoising could equally well be performed before the neural networks to further reduce the noise in the output.

In this study, we adapted the IVIM-NET physics-informed deep neural network to include tri-exponential fitting. We chose a physics informed loss function as it allows for training on patient data without inputting any ground-truth answers. Conventional loss functions are also available (Bertleff et al., 2017; Lee et al., 2021), but they either need to be trained on simulated data, or try to recreate the least-squares fit results in patient data. Therefore, we believe a physics-informed approach has more potential. We tried to minimize the changes to the already optimized IVIM-NET that we adapted the network from, to achieve comparable performance. However, tri-exponential fitting is more challenging and some adjustments were made to address this. The main differences were the implementation of a scheduler for the learning rate and splitting the network in three parts, which we found to improve the tri-exponential fit. Potentially, the network can be further improved in the future by adding spatial awareness with convolutional layers, such as done for e.g. DCE (Ulas et al., 2019).

In conclusion, the use of a tri-exponential IVIM model can be applied in patients with NAFLD and the IVIM<sub>3</sub>-NET can be used to produce high quality IVIM parameter maps, displaying less noise than a tri-exponential LSQ fit and providing strong correlations with liver histopathology scores, the current gold standard to diagnose and grade NAFLD.

## Data availability statement

The data analyzed in this study is subject to the following licenses/restrictions: The datasets generated during and/or analysed during the current study are available from the corresponding author on reasonable request. Requests to access these datasets should be directed to [m.a.troelstra@amsterdamumc.nl](mailto:m.a.troelstra@amsterdamumc.nl).

## Ethics statement

The studies involving human participants were reviewed and approved by the Institutional review board of the Academic Medical Centre. The patients/participants provided their written informed consent to participate in this study.

## Author contributions

Study design: OG-C, AN, MT, MN, AH, and JW; data acquisition: MT, A-MV, JW, AM, DZ, UB, MN, AH, AN, and OG-C; data analysis and interpretation: MT, JR, JV, AN, and OG-C; manuscript drafting: MT and OG-C All authors critically reviewed the manuscript. All authors approved the final version of the manuscript.

## Conflict of interest

The authors declare that the research was conducted in the absence of any commercial or financial relationships that could be construed as a potential conflict of interest.

## Publisher's note

All claims expressed in this article are solely those of the authors and do not necessarily represent those of their affiliated

organizations, or those of the publisher, the editors and the reviewers. Any product that may be evaluated in this article, or claim that may be made by its manufacturer, is not guaranteed or endorsed by the publisher.

## Supplementary material

The Supplementary Material for this article can be found online at: <https://www.frontiersin.org/articles/10.3389/fphys.2022.942495/full#supplementary-material>

## References

- Barbieri, S., Gurney-Champion, O. J., Klaassen, R., and Thoeny, H. C. (2020). Deep learning how to fit an intravoxel incoherent motion model to diffusion-weighted MRI. *Magn. Reson. Med.* 83 (1), 312–321. doi:10.1002/mrm.27910
- Bedossa, P. FLIP Pathology Consortium (2014). Utility and appropriateness of the fatty liver inhibition of progression (FLIP) algorithm and steatosis, activity, and fibrosis (SAF) score in the evaluation of biopsies of nonalcoholic fatty liver disease. *Hepatology* 60 (2), 565–575. doi:10.1002/hep.27173
- Bertleff, M., Domsch, S., Weingärtner, S., Zapp, J., O'Brien, K., Barth, M., et al. (2017). Diffusion parameter mapping with the combined intravoxel incoherent motion and kurtosis model using artificial neural networks at 3 T. *NMR Biomed.* 30 (12), e3833. doi:10.1002/nbm.3833
- Cercueil, J.-P., Petit, J.-M., Nougaret, S., Soyer, P., Fohlen, A., Pierredon-Foulongne, M.-A., et al. (2015). Intravoxel incoherent motion diffusion-weighted imaging in the liver: Comparison of mono-bi- and tri-exponential modelling at 3.0-T. *Eur. Radiol.* 25 (6), 1541–1550. doi:10.1007/s00330-014-3554-6
- Chevallier, O., Zhou, N., Cercueil, J., He, J., Loffroy, R., and Wang, Y. X. J. (2019). Comparison of tri-exponential decay versus bi-exponential decay and full fitting versus segmented fitting for modeling liver intravoxel incoherent motion diffusion MRI. *NMR Biomed.* 32 (11), 1–11. doi:10.1002/nbm.4155
- Chevallier, O., Wang, Y. X. J., Guillen, K., Pellegrinelli, J., Cercueil, J.-P., and Loffroy, R. (2021). Evidence of tri-exponential decay for liver intravoxel incoherent motion MRI: A review of published results and limitations. *Diagnostics* 11 (2), 379. doi:10.3390/diagnostics11020379
- Gilmore, I. T., Burroughs, A., Murray-Lyon, I. M., Williams, R., Jenkins, D., and Hopkins, A. (1995). Indications, methods, and outcomes of percutaneous liver biopsy in England and Wales: An audit by the British society of gastroenterology and the royal college of physicians of London. *Gut* 36 (3), 437–441. doi:10.1136/gut.36.3.437
- Gurney-Champion, O. J., Collins, D. J., Wetscherek, A., Rata, M., Klaassen, R., Van Laarhoven, H. W. M., et al. (2019). Principal component analysis for fast and model-free denoising of multi b-value diffusion-weighted MR images. *Phys. Med. Biol.* 64 (10), 105015. doi:10.1088/1361-6560/ab1786
- Kaandorp, M. P. T., Barbieri, S., Klaassen, R., Laarhoven, H. W. M., Crezee, H., While, P. T., et al. (2021). Improved unsupervised physics-informed deep learning for intravoxel incoherent motion modeling and evaluation in pancreatic cancer patients. *Magn. Reson. Med.* 86 (4), 2250–2265. doi:10.1002/mrm.28852
- Kleiner, D. E., Brunt, E. M., Van Natta, M., Behling, C., Contos, M. J., Cummings, O. W., et al. (2005). Design and validation of a histological scoring system for nonalcoholic fatty liver disease. *Hepatology* 41 (6), 1313–1321. doi:10.1002/hep.20701
- Koopman, T., Martens, R., Gurney-Champion, O. J., Yaqub, M., Lavini, C., Graaf, P., et al. (2021). Repeatability of IVIM biomarkers from diffusion-weighted MRI in head and neck: Bayesian probability versus neural network. *Magn. Reson. Med.* 85 (6), 3394–3402. doi:10.1002/mrm.28671
- Le Bihan, D., Breton, E., Lallemand, D., Aubin, M. L., Vignaud, J., and Laval-Jeantet, M. (1988). Separation of diffusion and perfusion in intravoxel incoherent motion MR imaging. *Radiology* 168 (2), 497–505. doi:10.1148/radiology.168.2.3393671
- Lee, W., Kim, B., and Park, H. (2021). Quantification of intravoxel incoherent motion with optimized b-values using deep neural network. *Magn. Reson. Med.* 86 (1), 230–244. doi:10.1002/mrm.28708
- Li, Y. T., Cercueil, J.-P., Yuan, J., Chen, W., Loffroy, R., and Wang, Y. X. J. (2017). Liver intravoxel incoherent motion (IVIM) magnetic resonance imaging: A comprehensive review of published data on normal values and applications for fibrosis and tumor evaluation. *Quant. Imaging Med. Surg.* 7 (1), 59–78. doi:10.21037/qims.2017.02.03
- Manjón, J. V., Coupé, P., Concha, L., Buades, A., Collins, D. L., and Robles, M. (2013). Diffusion weighted image denoising using overcomplete local PCA. *PLoS One* 8 (9), e73021–12. doi:10.1371/journal.pone.0073021
- Murphy, P., Hooker, J., Ang, B., Wolfson, T., Gamst, A., Bydder, M., et al. (2015). Associations between histologic features of nonalcoholic fatty liver disease (NAFLD) and quantitative diffusion-weighted MRI measurements in adults. *J. Magn. Reson. Imaging.* 41 (6), 1629–1638. doi:10.1002/jmri.24755
- Parthasarathy, G., Revelo, X., and Malhi, H. (2020). Pathogenesis of nonalcoholic steatohepatitis: An overview. *Hepatol. Commun.* 4 (4), 478–492. doi:10.1002/hep4.1479
- Parasin, M., Abralde, J. G., Liguori, E., Kok, B., and Mura, V. L. (2017). Intrahepatic vascular changes in non-alcoholic fatty liver disease: Potential role of insulin-resistance and endothelial dysfunction. *World J. Gastroenterol.* 23 (37), 6777–6787. doi:10.3748/wjg.v23.i37.6777
- R Core Team (2020). *R: A language and environment for statistical computing*. Vienna, Austria. [Internet].
- Riexinger, A. J., Martin, J., Rauh, S., Wetscherek, A., Pistel, M., Kuder, T. A., et al. (2019). On the field strength dependence of Bi- and triexponential intravoxel incoherent motion (IVIM) parameters in the liver. *J. Magn. Reson. Imaging.* 50 (6), 1883–1892. doi:10.1002/jmri.26730
- Riexinger, A., Martin, J., Wetscherek, A., Kuder, T. A., Uder, M., Hensel, B., et al. (2020). An optimized b-value distribution for triexponential intravoxel incoherent motion (IVIM) in the liver. *Magn. Reson. Med.* 85, 2095–2108. doi:10.1002/mrm.28582
- Seeff, L. B., Everson, G. T., Morgan, T. R., Curto, T. M., Lee, W. M., Ghany, M. G., et al. (2010). Complication rate of percutaneous liver biopsies among persons with advanced chronic liver disease in the HALT-C trial. *Clin. Gastroenterol. Hepatol.* 8 (10), 877–883. doi:10.1016/j.cgh.2010.03.025

Stefan, N., Häring, H. U., and Cusi, K. (2019). Non-alcoholic fatty liver disease: Causes, diagnosis, cardiometabolic consequences, and treatment strategies. *Lancet. Diabetes Endocrinol.* 7 (4), 313–324. doi:10.1016/S2213-8587(18)30154-2

Targher, G., Byrne, C. D., Lonardo, A., Zoppini, G., and Barbui, C. (2016). Non-alcoholic fatty liver disease and risk of incident cardiovascular disease: A meta-analysis. *J. Hepatol.* 65 (3), 589–600. doi:10.1016/j.jhep.2016.05.013

Troelstra, M. A., Witjes, J. J., Dijk, A., Mak, A. L., Gurney-Champion, O., Runge, J. H., et al. (2021). Assessment of imaging modalities against liver biopsy in nonalcoholic fatty liver disease: The Amsterdam NAFLD-NASH cohort. *J. Magn. Reson. Imaging.* 54, 1937–1949. doi:10.1002/jmri.27703

Ulas, C., Das, D., Thrippleton, M. J., Valdés Hernández, M. del C., Armitage, P. A., Makin, S. D., et al. (2019). Convolutional neural networks for direct inference of pharmacokinetic parameters: Application to stroke dynamic contrast-enhanced MRI. *Front. Neurol.* 9, 1147. doi:10.3389/fneur.2018.01147

Unal, E., Idilman, I. S., and Karçaaltuncaba, M. (2017). Multiparametric or practical quantitative liver MRI: Towards millisecond, fat fraction, kilopascal and function era. *Expert Rev. Gastroenterol. Hepatol.* 11 (2), 167–182. doi:10.1080/17474124.2017.1271710

Younossi, Z. M., Koenig, A. B., Abdelatif, D., Fazel, Y., Henry, L., and Wymer, M. (2016). Global epidemiology of nonalcoholic fatty liver disease-Meta-analytic assessment of prevalence, incidence, and outcomes. *Hepatology* 64 (1), 73–84. doi:10.1002/hep.28431